Inorg. Chem. **2008**, *47*, 9390−9399

Chiral II−VI Semiconductor Nanostructure Superlattices Based on an Amino Acid Ligand

Jean-Noël Rebilly, Paul W. Gardner, George R. Darling, John Bacsa, and Matthew J. Rosseinsky*

Department of Chemistry, University of Liverpool, Liverpool L69 7ZD, U.K.

Received June 14, 2008

Reaction of L-cysteine with $M(NO_3)_2 \cdot xH_2O$ (M = Cd, Zn) generates M(L-cysteinate), which feature one-dimensional substructures that can be viewed as fragments of bulk structures of CdS (rock salt high pressure phase) and ZnS (würtzite) because of the bridging modes accessible to the sulfur atom of L-cysteine. The MS substructures are arranged in a regular and periodic fashion within the crystal via the carboxylate function of L-cysteine. Considering the structural similarities with bulk materials, the optical properties of M(L-cysteinate) were studied and indicate blue shifts of the band gap of 2.59 eV (M = Cd, compared to CdS rock salt) and 1.37 eV (M = Zn, compared to ZnS würtzite) with respect to the bulk MS structures, due to the low dimensionality of the metal−sulfur arrangement. The chelating nature of the cysteine ligand imposes an unusual *mer* arrangement of three binding S moieties at Cd with a correspondingly high Cd coordination number in a chalcogenide-based material. Density of states calculations show strong electronic structure similarities with the bulk phases and rationalize the band gap changes.

Introduction

Nanostructured objects based on II−VI binary chalcogenides such as CdS or ZnS are widely studied for their applications in semiconductor systems including diodes, transistors, or photovoltaic devices.[1] The development of nanostructures of those materials allowed tuning the electronic and optical properties of such systems via the control of their dimensions.[2−15] Reduced dimension substructural units of these II−VI bulk phases can be organized by organic molecules introduced into the metal-chalcogenide network during solvothermal synthesis, affording a family of hybrid organic−inorganic systems in which the tetrahedral coordination characteristic of the bulk structures is retained.[16−22] The optical properties vary systematically as the bandwidth is reduced with respect to the bulk because of the reduced dimensions of the inorganic substructure, resulting in an increase of the observed band gap.

The aim of the present work is to generate purely molecule-based MS arrays formed by sulfur-containing ligands with structural relationships to fragments of the bulk II−VI semiconductors. The d^{10} ions are known to have a specific affinity for sulfur-containing ligands, as evidenced by the coordination of cysteine residues in the coordination

* To whom correspondence should be addressed. E-mail: m.j.rosseinsky@liv.ac.uk.

(1) Sze, S. M. *Semiconductor Devices, Physics and Technology*, 2nd ed.; Wiley: New York, 2001.
(2) Alivisatos, A. P. *Science* **1996**, *271*, 933–937.
(3) Steigerwald, M. L.; Alivisatos, A. P.; Gibson, J. M.; Harris, T. D.; Kortan, R.; Muller, A. J.; Thayer, A. M.; Duncan, T. M.; Douglass, D. C.; Brus, L. E. *J. Am. Chem. Soc.* **1988**, *110*, 3046–3050.
(4) Rossetti, R.; Hull, R.; Gibson, J. M.; Brus, L. E. *J. Chem. Phys.* **1985**, *82*, 552–559.
(5) Herron, N.; Wang, Y.; Eddy, M. M.; Stucky, G. D.; Cox, D. E.; Moller, K.; Bein, T. *J. Am. Chem. Soc.* **1989**, *111*, 530–540.
(6) Herron, N.; Wang, Y.; Eckert, H. *J. Am. Chem. Soc.* **1990**, *112*, 1322–1326.
(7) Spanhel, L.; Anderson, M. A. *J. Am. Chem. Soc.* **1990**, *112*, 2278–2284.
(8) Herron, N.; Calabrese, J. C.; Farneth, W. E.; Wang, Y. *Science* **1993**, *259*, 1426–1428.
(9) Horst, W. *Angew. Chem., Int. Ed.* **1993**, *32*, 41–53.
(10) Brenchley, M. E.; Weller, M. T. *Angew. Chem., Int. Ed. Engl.* **1993**, *32*, 1663–1665.
(11) Murray, C. B.; Norris, D. J.; Bawendi, M. G. *J. Am. Chem. Soc.* **1993**, *115*, 8706–8715.
(12) Murray, C. B.; Kagan, C. R.; Bawendi, M. G. *Science* **1995**, *270*, 1335–1338.
(13) Trindade, T.; O'Brien, P.; Pickett, N. L. *Chem. Mater.* **2001**, *13*, 3843–3858.
(14) Axtell, E. A., III.; Liao, J. H.; Pikramenou, Z.; Park, Y.; Kanatzidis, M. G. *J. Am. Chem. Soc.* **1993**, *115*, 12191–12192.
(15) Axtell, E. A., III.; Liao, J. H.; Pikramenou, Z.; Kanatzidis, M. G. *Chem.—Eur. J.* **1996**, *2*, 656–666.
(16) Huang, X.; Li, J.; Fu, H. *J. Am. Chem. Soc.* **2000**, *122*, 8789–8790.
(17) Huang, X.; Heulings, H. R.; Le, V.; Li, J. *Chem. Mater.* **2001**, *13*, 3754–3759.

10.1021/ic801097w CCC: $40.75
Published on Web 09/19/2008

sphere of Zn enzymes (zinc finger proteins)[23] or the affinity of Cd for metallothionein, cysteine, and glutathione.[24] According to the Cambridge Databank, several coordination polymers involving polymeric MS substructures based on thiolate ligands have been described with M = Cd,[25−47] but only a few with M = Zn.[48,49] Natural aminoacids have recently been shown to be useful ligands for the construction of metal-organic frameworks,[50−63] and we therefore investigated the coordination potential of L-cysteine with metal salts under solvothermal conditions. Herein, we report the synthesis and structures of two three-dimensional (3D) chiral materials Cd(L-cysteinate) **1** and Zn(L-cysteinate) **2**. The single polydentate cysteine ligand bearing a thiolate function affords two-atom thick one-dimensional (1D) fragments of the high pressure rock salt phase of CdS (in **1**) and the ambient pressure würtzite phase of ZnS (in **2**). The capping ligand imposes both the 1D nature of the substructure and the local coordination at the metal and organizes these substructures in a periodic and regular fashion within the crystals via its nonsulfur bridging functions. **1** is notable for the *mer* arrangement of the three coordinating S moieties, which is not accessible at ambient pressure in CdS and results from the six-coordination of Cd imposed by the chelating ligand. Electronic structure calculations show that these extended molecular systems retain the characteristics of the electronic structure of the corresponding bulk sulfide phases.

Experimental Section

Single Crystal X-ray Diffraction. The single-crystal diffraction data were collected on stations 9.8 and 16.2SMX of the Synchrotron Radiation Source at Daresbury Laboratory which utilize a Bruker-Nonius APEXII CCD area detector and D8 diffractometer at an X-ray wavelength of 0.6911 Å (1) on station 16.2SMX, and 0.6710 Å (2), on station 9.8. Data were recorded at 150 K. The reflection data were integrated using the APEX II software.[64] The data were corrected for absorption, decay, and other systematic errors using SADABS V2008-1.[65] The structure was solved (by direct methods) and refined using SHELX-97.[66]

Diffuse Reflectance Measurements. Optical diffuse reflectance spectra were recorded with a Perkin-Elmer Lambda 650 S double beam double monochromator spectrophotometer at room temperature. Data were collected in the 190−900 nm range in the reflectance mode. Barium sulfate was used as a standard of 100% reflectance.

Luminescence Measurements. Emission spectra were recorded at room temperature with a Perkin-Elmer LS 55 fluorescence spectrometer. Powder samples were placed in a powder holder equipped with a synthetic fused silica window. Samples were irradiated between 200 and 260 nm. Emission spectra were collected in the range 200−800 nm.

Thermal Analysis. Thermogravimetric analysis (TGA) data were recorded using a Seiko S−II instrument.

(18) Huang, X.; Li, J.; Zhang, Y.; Mascarenhas, A. *J. Am. Chem. Soc.* **2003**, *125*, 7049–7055.
(19) Huaxiang, F.; Jing, L. *J. Chem. Phys.* **2004**, *120*, 6721–6725.
(20) Huang, X.; Li, J. *J. Am. Chem. Soc.* **2007**, *129*, 3157–3162.
(21) Fluegel, B.; Zhang, Y.; Mascarenhas, A.; Huang, X.; Li, J. *Phys. Rev. B: Condens. Matter* **2004**, *70*, 205308.
(22) Yong, Z.; Dalpian, G. M.; Fluegel, B.; Su-Huai, W.; Mascarenhas, A.; Huang, X. Y.; Li, J.; Wang, L. W. *Phys. Rev. Lett.* **2006**, *96*, 026405.
(23) Rosenberg, U. B.; Schröder, C.; Preiss, A.; Kienlin, A.; Côté, S.; Riede, I.; Jäckle, H. *Nature* **1986**, *319*, 336.
(24) Singhal, R. K. ; Anderson, M. E. ; Meister, A. *FASEB J.* **1987**, *1*, 220–223.
(25) Dance, I. G.; Scudder, M. L.; Secomb, R. *Inorg. Chem.* **1983**, *22*, 1794.
(26) Bürgi, H.-B. *Helv. Chim. Acta* **1974**, *57*, 513–519.
(27) Craig, D.; Dance, I. G.; Garbutt, R. *Angew. Chem., Int. Ed. Engl.* **1986**, *25*, 165–166.
(28) Lang, E. S.; de Oliveira, G. M.; Casagrande, G. A.; Vazquez-Lopez, E. M. *Inorg. Chem. Commun.* **2003**, *6*, 1297.
(29) van Poppel, L. H. ; Groy, T. L. ; Caudle, M. T. *Inorg. Chem.* **2004**, *43*, 3180.
(30) Dance, I. G.; Garbutt, R. G.; Craig, D. C.; Scudder, M. L. *Inorg. Chem.* **1987**, *26*, 4057.
(31) Dance, I. G.; Garbutt, R. G.; Craig, D. C.; Scudder, M. L.; Bailey, T. D. *Chem. Commun.* **1987**, 1184.
(32) Casals, I.; Gonzalez-Duarte, P.; Sola, J.; Font-Bardia, M.; Solans, J.; Solans, X. *J. Chem. Soc., Dalton Trans.* **1987**, 2391.
(33) Dubler, E.; Gyr, E. *Inorg. Chem.* **1988**, *27*, 1466.
(34) Sousa-Pedrares, A.; Romero, J.; Garcia-Vazquez, J. A.; Duran, M. L.; Casanova, I.; Sousa, A. *Dalton Trans.* **2003**, 1379.
(35) Fleischer, H.; Dienes, Y.; Mathiasch, B.; Schmitt, V.; Schollmeyer, D. *Inorg. Chem.* **2005**, *44*, 8087.
(36) Hursthouse, M. B.; Khan, O. F. Z.; Mazid, M.; Motevalli, M.; O'Brien, P. *Polyhedron* **1990**, *9*, 541–544.
(37) Eichhofer, A.; Buth, G. *Eur. J. Inorg. Chem.* **2005**, 4160.
(38) Fu, A.-Y.; Wang, D.-Q.; Xing, J.-X. *Acta Crystallogr., Sect. E: Struct. Rep. Online* **2005**, *61*, m2115.
(39) Bayon, J. C.; Brianso, M. C.; Brianso, J. L.; Duarte, P. G. *Inorg. Chem.* **1979**, *18*, 3478–3482.
(40) Marsh, R. E.; Schomaker, V. *Inorg. Chem.* **1981**, *20*, 299.
(41) Cai, Z. X.; Yang, H.; Zhang, Y.; Yan, X. P. *Anal. Chim. Acta* **2006**, *559*, 234–239.
(42) Bharara, M. S.; Kim, C. H.; Parkin, S.; Atwood, D. A. *Polyhedron* **2005**, *24*, 865.
(43) Amo-Ochoa, P.; Rodriguez-Tapiador, M. I.; Castillo, O.; Olea, D.; Guijarro, A.; Alexandre, S. S.; Gomez-Herrero, J.; Zamora, F. *Inorg. Chem.* **2006**, *45*, 7642.
(44) Castro, J. A.; Romero, J.; Garcia-Vazquez, J. A.; Sousa, A.; Zubieta, J.; Chang, Y. *Polyhedron* **1996**, *15*, 2741.
(45) Dance, I. G.; Garbutt, R. G.; Scudder, M. L. *Inorg. Chem.* **1990**, *29*, 1571–1575.
(46) Vossmeyer, T.; Reck, G.; Katsikas, L.; Haupt, E. T. K.; Schulz, B.; Weller, H. *Inorg. Chem.* **1995**, *34*, 4926–4929.
(47) Zhang, Q.; Bu, X.; Zhang, J.; Wu, T.; Feng, P. *J. Am. Chem. Soc.* **2007**, *129*, 8412.
(48) Dance, I. G. *J. Am. Chem. Soc.* **1980**, *102*, 3445.
(49) Muller, B.; Schneider, A.; Tesmer, M.; Vahrenkamp, H. *Inorg. Chem.* **1999**, *38*, 1900.
(50) Ingleson, M. J.; Bacsa, J.; Rosseinsky, M. J. *Chem. Commun.* **2007**, 3036–3038.
(51) Vaidhyanathan, R.; Bradshaw, D.; Rebilly, J. N.; Barrio, J. P.; Gould, J. A.; Berry, N. G.; Rosseinsky, M. J. *Angew. Chem., Int. Ed.* **2006**, *45*, 6495–6499.
(52) Anokhina, E. V.; Jacobson, A. J. *J. Am. Chem. Soc.* **2004**, *126*, 3044–3045.
(53) Anokhina, E. V.; Go, Y. B.; Lee, Y.; Vogt, T.; Jacobson, A. J. *J. Am. Chem. Soc.* **2006**, *128*, 9957–9962.
(54) Ingleson, M. J.; Perez Barrio, J.; Bacsa, J.; Dickinson, C.; Park, H.; Rosseinsky, M. J. *Chem. Commun.* **2008**, 1287–1289.
(55) Antolini, L.; Menabue, L.; Pellacani, G. C.; Marcotrigiano, G. *Dalton Trans.* **1982**, 2541–2543.
(56) Schmidbaur, H.; Bach, I.; Riede, J.; Muller, G.; Helbig, J.; Hopf, G. *Chem. Ber.* **1988**, 121.
(57) Doyne, T. H.; Pepinsky, R.; Watanabe, T. *Acta Crystallogr.* **1957**, 10.
(58) Zhang, Y.; Saha, M. K.; Bernal, I. *CrystEngComm* **2003**, *5*, 34.
(59) Mizutani, M.; Maejima, N.; Jitsukawa, K.; Masuda, H.; Einaga, H. *Inorg. Chim. Acta* **1998**, *283*, 105.
(60) Flook, R. J.; Freeman, H. C.; Scudder, M. L. *Acta Crystallogr., Sect. B* **1977**, *33*, 801.
(61) Gramaccioli, C. M. *Acta Crystallogr.* **1966**, *21*, 600.
(62) Yukawa, Y.; Inomata, Y.; Takeuchi, T. *Bull. Chem. Soc. Jpn.* **1983**, *56*, 2125.
(63) Xie, Y.; Wu, H.-H.; Yong, G.-P.; Wang, Z.-Y.; Fan, R.; Li, R.-P.; Pan, G.-Q.; Tian, Y.-C.; Sheng, L.-S.; Pan, L.; Li, J. *J. Mol. Struct.* **2007**, *833*, 88.
(64) *APEX II*; Bruker AXS Inc.: Madison, WI, 2005.
(65) *SADABS Version 2008−2*; Bruker AXS Inc.: Madison, WI, 2007.
(66) Sheldrick, G. M., *SHELX97*; University of Göttingen: Göttingen, Germany, 1997.

X-ray Powder Diffraction. X-ray powder diffraction data were collected with Co $K\alpha_1$ radiation with a Panalytical X'pert Pro Multi-Purpose diffractometer in reflection geometry.

Synthesis. L-cysteine, $Zn(NO_3)_2 \cdot 6H_2O$, and $Cd(NO_3)_2 \cdot 4H_2O$ were purchased from Aldrich.

Cd(L-cysteinate) 1. $Cd(NO_3)_2 \cdot 4H_2O$ (0.095 g, 0.308 mmol) and L-cysteine (0.035 g, 0.289 mmol) were mixed in water (6 mL) in a 23 mL Teflon liner. A solution of sodium hydroxide (2 mol·L^{-1}) was added dropwise under stirring to reach an initial pH of 5.85. The resulting mixture was reacted at 80 °C for 24 h. The crude product was filtered and washed thoroughly with water, giving a white microcrystalline phase pure bulk powder. Yield: 78%. Elemental analysis (%) for Cd(L-cysteinate) ($C_3H_5CdNO_2S$), M = 232.9, calculated C 15.56, H 2.18, N 6.05, Cd 48.55; found C 15.49, H 2.16, N 6.07, Cd 47.95. Single crystals of **1** of suitable size for X-ray diffraction were obtained, alongside a yellow amorphous side product, from the reaction of $Cd(NO_3)_2 \cdot 4H_2O$ (0.095 g, 0.308 mmol), L-cysteine (0.035 g, 0.289 mmol), and sodium hydrogencarbonate (0.048 g, 0.578 mmol) in water/methanol (3 mL/3 mL) in a 23 mL Teflon liner at 100 °C for 18 h.

Zn(L-cysteinate) 2. The white microcrystalline phase pure material is obtained by replacing $Cd(NO_3)_2 \cdot 4H_2O$ by $Zn(NO_3)_2 \cdot 6H_2O$ (0.092 g, 0.308 mmol) in the procedure described for the synthesis of phase pure bulk **1**. Yield: 73%. Elemental analysis calcd (%) for Zn(L-cysteinate) ($C_3H_5ZnNO_2S$), M = 182.9, calcd C 19.53, H 2.73, N 7.59, Zn 35.44); found C 19.51, H 2.69, N 7.55, Zn 34.89.

Single crystals of **2** of suitable size for X-ray diffraction were obtained (as a non-pure phase) by replacing $Cd(NO_3)_2 \cdot 6H_2O$ by $Zn(NO_3)_2 \cdot 6H_2O$ (0.092 g, 0.308 mmol) in the procedure described for the isolation of single crystals of **1**.

Density of States (DOS) Calculations. Calculations were performed in two parts. Initially, structures were optimized using the plane-wave basis set density-functional theory (DFT) electronic structure program VASP (v4.6.26). For the calculations reported here the Generalized Gradient Approximation of Perdew and Wang (GGA-PW91) was used for geometry optimization with atoms represented by the projector augmented wave (PAW) potentials with a plane-wave cutoff energy of 500 eV for all systems. In the case of **1**, the atoms were first relaxed before relaxing the cell parameters whereas for bulk würtzite CdS both relaxations were performed simultaneously.

DFT is known to underestimate band gaps and hence another suitable method was sought to provide a more accurate answer. Hybrid Hartree−Fock plus DFT functionals add a contribution of Fock exchange to the standard DFT and have been demonstrated to yield improved band-gaps compared to standard DFT and Hartree−Fock.[67−69] Specifically, comparisons between PBE (Perdew−Burke−Ernzerhof) and the hybrid PBE0, B3LYP (Becke, three-parameter, Lee−Yang−Parr), and HSE03 (Heyd, Scuseria, Ernzerhof) showed that PBE0 and HSE03 provide an improved description of the band gaps compared to conventional DFT. HSE03 and PBE0[68,70] are implemented in the most recent (unreleased) version of VASP (v5.1.28); however, these functionals are too computationally expensive to be used in standard electronic structure geometry optimization calculations on large systems. To obtain more reasonable estimates of the band gaps, we have therefore used the standard DFT for geometry optimization, subsequently running VASP v5.1.28 to obtain the self-consistent electronic structure with the HSE03 functional.

Table 1. Crystal Data and Structure Refinement for **1** and **2**[a]

	1	**2**
empirical formula	$C_3H_5CdNO_2S$	$C_3H_5NO_2SZn$
M	231.54	184.51
crystal description	colorless prism	colorless prism
size/mm^3	0.05 × 0.04 × 0.03	0.04 × 0.03 × 0.02
crystal system	orthorhombic	orthorhombic
space group	$P2_12_12_1$	$P2_12_12_1$
a /Å	5.6307(11)	6.025(3)
b /Å	9.483(2)	8.838(5)
c /Å	9.542(2)	9.402(5)
V /Å^3	509.48(17)	500.7(5)
Z	4	4
D_c /g/cm^3	3.019	2.448
F_{000}	440	368
radiation	synchrotron	synchrotron
λ /Å	0.691	0.671
T /K	150(2)	150(2)
$2\theta_{max}$ /deg	54.9	61.1
no. reflections collected	3339, 1161 unique	3106, 1475 unique
R_{int}	0.0239	0.1118
final GOF	1.054	0.915
R1	0.0183	0.0650
wR2	0.0411	0.1292
no. parameters, restraints	93, 5	73, 0
μ /mm^{-1}	4.581 mm^{-1}	4.667 mm^{-1}
Flack parameter	−0.03(4)	0.02(6)

[a] The structures were refined to F_o^2, *R* indices based on reflections with $I > 2\sigma(I)$, and all reflections were used in the least-squares calculations.

Results and Discussion

Crystal Structure Description. White crystals of Cd(L-cysteinate) **1** suitable for single crystal diffraction are grown from solvothermal reaction of a mixture of $Cd(NO_3)_2 \cdot 4H_2O$ with L-cysteine and sodium hydrogencarbonate in a water/methanol mixture at 100 °C for 18 h. Under those conditions, they form alongside a yellow powder, probably because of the partial decomposition of cysteine to sulfide in situ and the subsequent formation of CdS compounds.[71] Milder conditions (80 °C, 24 h, and pH adjusted to 5.85 in pure water) prevent the decomposition of cysteine and allow isolation of **1** as a pure phase (Supporting Information, Figure S1). **1** crystallizes in the chiral space group $P2_12_12_1$ (a = 5.6307(11) Å, b = 9.4827(19) Å, c = 9.5418(19)Å, Table 1). The structure (Figure 1) is built from a 1D ladder arrangement of cadmium and sulfur atoms arising from the bridging of Cd centers by the thiol moiety of cysteine. These 1D units are held together in a regular fashion via the carboxylate function of cysteine which binds to Cd centers of two neighboring ladders via its two oxygens. The coordination sphere of cadmium is a distorted octahedron, with one L-cysteinate ligand acting as a tridentate capping ligand in a *fac* fashion via its amine, carboxylate, and thiolate groups. The bite angles of cysteinate are O2−Cd1A−N1 = 68.82°, O2−Cd1A−S1A = 79.95°, and N1−Cd1A−S1A = 72.60°. The bond lengths to the three donor atoms from the chelating ligand are Cd1A−N1 = 2.316 Å, Cd1A−O2 = 2.453 Å, and Cd1A−S1A = 2.947 Å (Figure 1a, Table 2).

(67) Marsman, M.; Paier, J.; Stroppa, A.; Kresse, G. *J. Phys.: Condens. Matter* **2008**, *20*, 064201.
(68) Paier, J.; Marsman, M.; Hummer, K.; Kresse, G.; Gerber, C.; Ángyán, J. G. *J. Chem. Phys.* **2006**, *124*, 154709.
(69) Muscat, J.; Wander, A.; Harrison, N. M. *Chem. Phys. Lett.* **2001**, *342*, 397.
(70) Paier, J.; Hirschl, R.; Marsman, M.; Kresse, G. *J. Chem. Phys.* **2005**, *122*, 234102.
(71) Xiong, S.; Xi, B.; Wang, C.; Zou, G.; Fei, L.; Wang, W.; Qian, Y. *Chem.—Eur. J.* **2007**, *13*, 3076–3081.

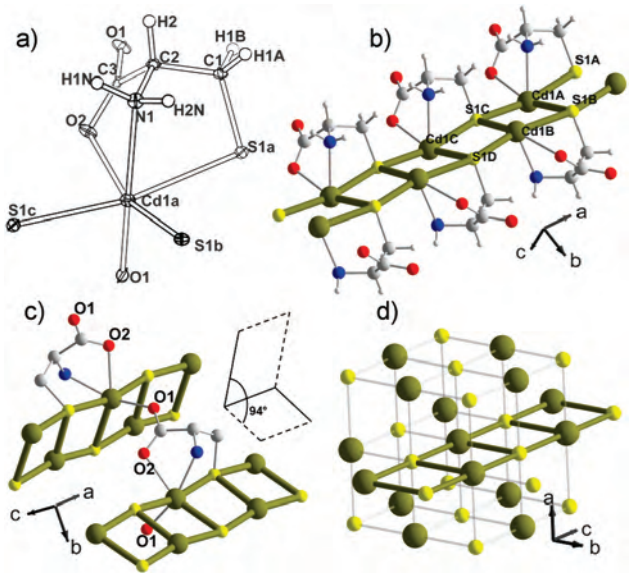

Figure 1. (a) Coordination sphere of Cd in **1**; (b) The Cd−S ladder substructure which is the fundamental structural unit of **1** (in green). Its direction corresponds to the 2_1 screw axis along *a*. The Cd1B−S1C−Cd1A angles are 87.92° and the S1C−Cd1A−S1B angles are 97.30°. (c) View of two neighboring ladders in **1** linked by the carboxylate function of cysteine. (d) View of the structure of the high pressure (40 kbar) rock salt phase of cadmium sulfide. A fragment of the bulk that compares to the CdS ladder substructure of **1** is highlighted with thick bonds. Cd, green; S, yellow; C, gray; O, red; N, dark blue; H, white.

Table 2. Selected Bond Lengths (Å) and Angles (deg) for **1**[a]

Cd(1)−S(1)	2.7110(11)	Cd(1)−O(1)$^{\#3}$	2.232(3)
Cd(1)−S(1)$^{\#1}$	2.9470(11)	Cd(1)−O(2)$^{\#1}$	2.453(2)
Cd(1)−N(1)$^{\#1}$	2.316(3)	Cd(1)−S(1)$^{\#2}$	2.6006(11)
S(1)−C(1)	1.831(3)	O(1)−C(3)	1.270(4)
O(2)−C(3)	1.250(4)	N(1)−C(2)	1.472(5)
S(1)−Cd(1)−S(1)$^{\#1}$	168.74(2)	S(1)−Cd(1)−O(2)$^{\#1}$	89.41(6)
S(1)−Cd(1)−N(1)$^{\#1}$	100.23(7)	S(1)−Cd(1)−S(1)$^{\#2}$	97.30(3)
S(1)−Cd(1)−O(1)$^{\#3}$	89.72(9)	S(1)$^{\#1}$−Cd(1)−O(2)$^{\#1}$	79.95(6)
S(1)$^{\#1}$−Cd(1)−N(1)$^{\#1}$	72.60(7)	S(1)$^{\#1}$−Cd(1)−S(1)$^{\#2}$	91.70(3)
S(1)$^{\#1}$−Cd(1)−O(1)$^{\#3}$	93.63(9)	O(2)$^{\#1}$−Cd(1)−N(1)$^{\#1}$	68.82(9)
S(1)$^{\#2}$−Cd(1)−O(2)$^{\#1}$	160.62(7)	O(1)$^{\#3}$−Cd(1)−O(2)$^{\#1}$	88.51(10)
S(1)$^{\#2}$−Cd(1)−N(1)$^{\#1}$	92.04(7)	O(1)$^{\#3}$−Cd(1)−N(1)$^{\#1}$	154.93(10)
S(1)$^{\#2}$−Cd(1)−O(1)$^{\#3}$	109.60(8)	Cd(1)−S(1)−Cd(1)$^{\#4}$	168.74(3)
Cd(1)−S(1)−Cd(1)$^{\#5}$	87.92(3)	Cd(1)$^{\#4}$−S(1)−C(1)	93.41(13)
Cd(1)$^{\#5}$−S(1)−C(1)	106.38(12)	Cd(1)$^{\#4}$−S(1)−Cd(1)$^{\#5}$	83.08(3)
S(1)−C(1)−C(2)	113.8(3)	N(1)−C(2)−C(1)	109.8(3)
N(1)−C(2)−C(3)	110.7(3)	O(1)−C(3)−C(2)	114.2(3)
O(2)−C(3)−C(2)	119.8(3)	O(1)−C(3)−O(2)	126.0(4)

[a] Symmetry transformations used to generate equivalent atoms: $^{\#1}$ $x+1, y, z$; $^{\#2}$ $x+1/2, -y+1/2, -z+1$; $^{\#3}$ $-x+1, y-1/2, -z+1/2$; $^{\#4}$ $x-1, y, z$; $^{\#5}$ $x-1/2, -y+1/2, -z+1$; $^{\#6}$ $-x+1, y+1/2, -z+1/2$.

The coordination sphere is completed by two sulfur atoms from cysteine ligands which chelate two neighboring Cd centers in the chain and one oxygen atom from the carboxylate of a cysteine forming a neighboring chain. As a result, the three sulfur atoms at a Cd center are arranged in a *mer* fashion and the two oxygen atoms are *cis*. (Figure 1a).

Each sulfur atom connects three Cd centers in a T-shape pattern, and each Cd center is bound to three S atoms in a *mer* fashion: thus, considering only Cd−S bonds, cadmium also displays T-shape coordination. As a consequence, the bonding motif creates a ladder shaped Cd−S substructure along the *a* axis, with Cd and S atoms alternating as the three-connected nodes of the ladder. The Cd1A−S1B bond corresponding to the step of the ladder is the shortest with a

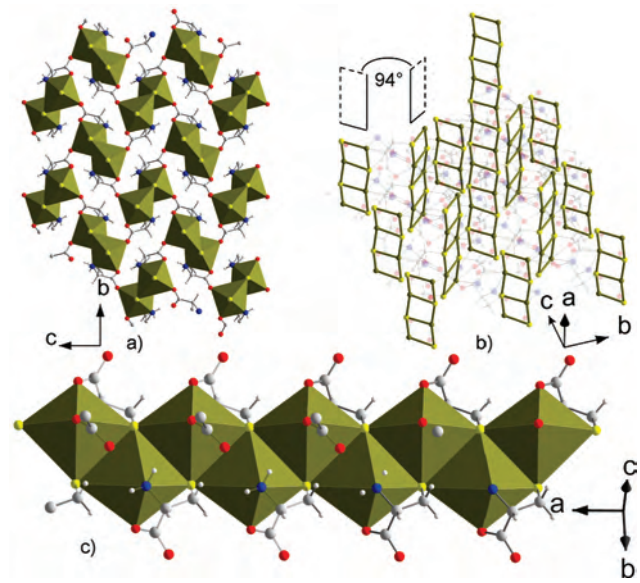

Figure 2. (a) View of the 3D structure of **1** in the (b,c) plane. All ladders (polyhedral representation) are oriented along the *a* axis and share no edges or corners with each other. Octahedra are centered on Cd atoms; (b) View displaying the arrangement of ladders along *a* in **1**. The amino acid backbone is made partially transparent for clarity. Cd−S bonds generate the ladders and are highlighted in bold green. From a symmetry point of view, neighboring ladders are generated from the original one by 2_1 screw axes along *b* and *c*. As a consequence, all ladders have the same principal axis (*a* axis), but as the average plane of the CdS substructure makes an angle of 43° with the (*a*, *c*) plane, those 2_1 axes create angles of 94° between neighboring ladders. (c) Polyhedral representation of a single ladder, showing that each Cd center shares two *cis* edges with its two CdL_6 neighbors, forming a 1D arrangement. Octahedra are centered on Cd atoms; S, yellow; C, gray; O, red; N, dark blue; H, white.

length of 2.600 Å. Two different bond lengths occur along the axis of the ladder. The chelate Cd1A−S1A bond (2.947 Å) is long but within an acceptable bonding range when compared to other thiolate-based cadmium coordination polymers,[34,36,72] whereas the Cd1A-S1C contact bridging the Cd(cysteinate) moieties along the *a* axis is shorter (2.711 Å).

The 1D CdS ladder substructure is almost planar as the S1D−Cd1B−S1C−Cd1A angle is 173.0° (Figure 1b). It forms by edge-sharing of neighboring Cd octahedra. Two adjacent S−S edges connect one Cd to its two neighbors, generating a 1D arrangement (Figure 2c), which is a restricted fragment of the rock salt structure, in which all octahedral edges are shared. The large S donor atom can play this edge-bridging role unlike the smaller first row donor atoms. The nitrogen atom (N1) and one of the oxygen atoms of the carboxylate function (O2, *cis* to N1) of cysteine are both monodentate to Cd. The last site in the cadmium coordination sphere (*trans* to N1) is occupied by the O1 oxygen atom of a carboxylate belonging to a neighboring ladder. These three atoms prevent any further edge-sharing for the Cd octahedron and thus prevent the substructure from extending in the (*b,c*) plane (Figure 2a). The ladders mutually saturate the coordination sphere of their constituent metal centers by connecting to each other via bridging carboxylates. Each ladder acts as a ligand (via its O1 atoms) toward two of its neighboring ladders (Figure 2a). Reciprocally, two other

(72) Lopez-Torres, E.; Mendiola, M. A. *Polyhedron* **2005**, *24*, 1435–1444.

neighboring ladders will complete the coordination sphere of the Cd centers in this first one, resulting in the connection of each 1D substructure to four neighbors by the carboxylate units, which are bridging in a 1,3 "syn, anti" mode and connect the ladders together within the 3D structure (Figure 1c and Figure 2a). As O1 and O2 are *cis* to each other, a carboxylate group forms a Cd−O2 chelate bond with one ladder that lies almost in the mean plane of the CdS ladder substructure and a Cd−O1 bridging bond with a second ladder that is forced to be almost perpendicular to the mean plane of that second CdS substructure, (Figure 1c). As a consequence, two neighboring 1D CdS substructures form an angle of 94° (Figures 1c and 2b). The Cd coordination sphere is very distorted as this second oxygen generates angles of O1−Cd1A−N1 = 154.93° and O1−Cd1A−S1B = 109.60° (Figure 1a).

The array of Cd−S bonds which form the core structural feature of **1** can be related to the structures of both the ambient and high pressure forms of bulk CdS. The ladder-shaped CdS array in **1** is a fragment present in the high pressure rock salt CdS phase (Figure 1d). The Cd1B−S1C−Cd1A (87.92°) and S1C−Cd1A−S1B (97.30°) angles are close to 90° found in the bulk phase. The mean Cd−S bond length (2.752 Å) is also close to the rock salt value of 2.715 Å (at 40 kbar). The length difference between the bonds oriented along the *a* axis (2.947 Å for the chelate bond Cd1A−S1A, 2.711 Å for the bridging bond S1C−Cd1A, Figure 1b) indicates a certain degree of distortion. If Cd1A−S1A is not considered as forming part of the Cd coordination sphere, the CdS substructure appears as a zigzag chain compressed along the *a* axis. This is a highly distorted fragment of the würtzite structure of CdS (Supporting Information, Figure S1). The bond lengths in this bulk phase are significantly shorter (2.526 and 2.540 Å), and cadmium is only four coordinate in würtzite CdS, making the high pressure CdS phase analogy more appropriate for **1** where the Cd coordination number is six. The higher coordination number at ambient pressure in **1** compared to CdS can be understood as favored by the smaller size of the first row N and O ligands also involved in bonding to Cd in **1**, compared to the CdS phases where S is the only ligand. The CdS substructures in **1** are thus best described as slightly distorted 1D fragments of the high pressure phase (rock salt) of CdS. It is worth noting that this *mer* arrangement of three S ligands is rare in cadmium compounds, as the corresponding CdS bulk phase is not stable at ambient pressure. Most cadmium sulfide[73,74] (or cadmium thiolate[25−47]) systems display a würtzite-like connectivity. The fact that the Cd1A−S1A bond (2.947 Å) is the longest of all the Cd−S bonds in **1** suggests that the presence of S1A in the coordination sphere of Cd1A is only maintained because of the chelate effect. If the thiol group was not connected to the rest of the amino acid backbone, relaxation along the *a* axis could occur to allow the 1D CdS substructure to adopt a more favorable würtzite-like arrangement (Supporting Information, Figure S2). The specific "rock salt" 1D CdS pattern in **1**, characterized by a *mer* arrangement of three S ligands producing an edge-sharing chain, is thus enforced by the chelate effect of the ligand.

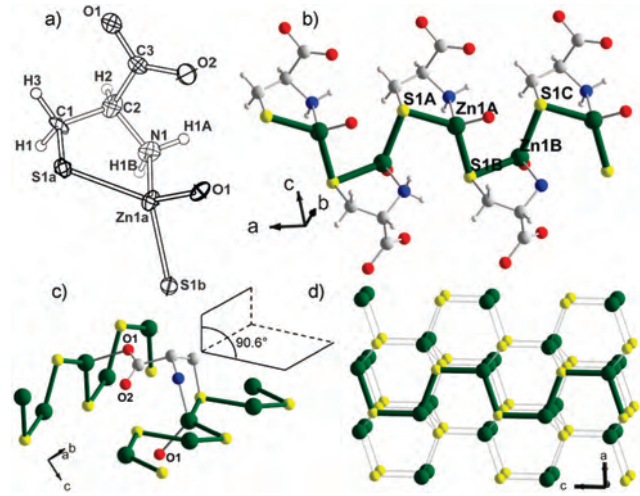

Figure 3. (a) Coordination sphere of Zn in **2**. (b) Zigzag 1D Zn−S substructure in **2** (in dark green); (c) two neighboring chains are bridged by the carboxylate function; the mean planes of the two chains are at an angle of 90.6°. (d) View of the structure of the würtzite phase of bulk ZnS. A comparable fragment to the ZnS chain substructure in **2** is highlighted with thick bonds. Zn, dark green; S, yellow; C, gray; O, red; N, dark blue; H, white.

White crystals of Zn(L-cysteinate) **2** are grown from solvothermal reactions of a mixture of $Zn(NO_3)_2 \cdot 6H_2O$ with L-cysteine and sodium hydrogencarbonate in a water/methanol mixture at 120 °C for 18 h. This temperature is necessary to grow single crystals with suitable size for X-ray diffraction but also leads to the formation of a yellowish powder, attributed, as in the case of **1**, to the partial decomposition of cysteine and the subsequent formation of sulfide compounds. Milder temperature conditions and pH adjustment with sodium hydroxide permits the isolation of **2** as a microcrystalline pure phase. **2** crystallizes in the chiral space group $P2_12_12_1$ (a = 6.025(3), b = 8.838(5), c = 9.402(5) Å, Table 1). The major structural difference from **1** stems from the reduced coordination number of the smaller Zn, which is four coordinate in a tetrahedral environment in **2**. This changes the nature of the 1D ZnS structural subunit formed by L-cysteine, which in **2** is only bidentate via the N and S atoms toward one Zn center (Figure 3a). The extended structural unit defining **2** is a zigzag alternating Zn−S chain, where the second S in the Zn coordination sphere is generated by the bridging thiolate function of a cysteinate that is bidentate to the neighboring Zn in the chain (Figure 3b). In contrast to **1**, the carboxylate group does not bind to the Zn atom locked into this chain subunit by the S and N functions, and thus cysteine is not involved in the tridentate chelate binding mode. Instead, the carboxylate group is oriented outward away from the chain and binds in a monodentate fashion to a second Zn center in a neighboring chain. The Zn (N, O, 2S) tetrahedral environment is thus defined by bidentate (N,S) and bridging S from two cysteine ligands defining the chain and O from the carboxylate of a cysteine that defines a neighboring chain. The resulting chain is much

(73) Müller, W. J.; Löffler, G. *Angew. Chem.* **1933**, *46*, 538–539.
(74) Stevenson, A. W.; Milanko, M.; Barnea, Z. *Acta Crystallogr., Sect. B: Struct. Sci.* **1984**, *40*, 521–530.

Table 3. Selected Bond Lengths (Å) and Angles (deg) for **2**[a]

Zn(1)−S(1)	2.370(4)	Zn(1)−N(1)	2.056(9)
Zn(1)−O(1)$^{\#1}$	1.995(8)	Zn(1)−S(1)$^{\#2}$	2.348(4)
S(1)−C(1)	1.856(10)	O(1)−C(3)	1.261(12)
O(2)−C(3)	1.277(15)	N(1)−C(2)	1.471(15)
S(1)−Zn(1)−N(1)	87.1(3)	S(1)−Zn(1)−O(1)$^{\#1}$	111.5(2)
S(1)−Zn(1)−S(1)$^{\#2}$	124.27(11)	O(1)$^{\#1}$−Zn(1)−N(1)	125.2(3)
S(1)$^{\#2}$−Zn(1)−N(1)	102.7(3)	S(1)$^{\#2}$−Zn(1)−O(1)$^{\#1}$	106.6(2)
Zn(1)−S(1)−C(1)	94.5(4)	Zn(1)−S(1)−Zn(1)$^{\#3}$	92.75(11)
Zn(1)$^{\#3}$−S(1)−C(1)	106.9(3)	Zn(1)$^{\#4}$−O(1)−C(3)	108.0(7)
Zn(1)−N(1)−C(2)	112.8(7)	S(1)−C(1)−C(2)	113.9(8)
N(1)−C(2)−C(1)	110.2(9)	N(1)−C(2)−C(3)	107.9(9)
O(1)−C(3)−C(2)	117.9(10)	O(2)−C(3)−C(2)	117.3(9)
O(1)−C(3)−O(2)	124.7(9)		

[a] Symmetry transformations used to generate equivalent atoms: $^{\#1}$ $-x + 3/2, -y, z + 1/2$; $^{\#2}$ $x - 1/2, -y + 1/2, -z + 2$; $^{\#3}$ $x + 1/2, -y + 1/2, -z + 2$; $^{\#4}$ $-x + 3/2, -y, z - 1/2$.

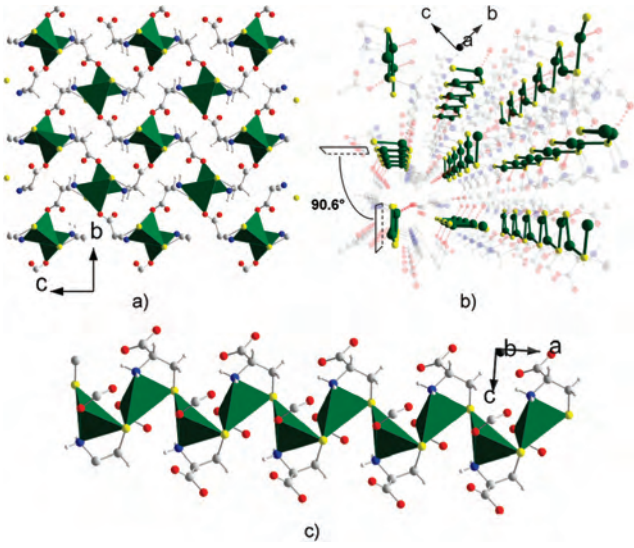

Figure 4. (a) Views of the 3D structure of **2** in the (b,c) plane. The pendant carboxylates connect one chain to its four neighbors.; (b) views of the 3D structure of **2** showing the arrangement of chains along the *a* axis. The mean plane of a chain forms a 90.6° angle with that of its four neighboring chains. The aminoacid backbone is made partially transparent for clarity. Zn−S bonds generate the chains and are highlighted in bold green. (c) Tetrahedral representation of a chain, showing that the 1D ZnS substructure is generated by corner-sharing tetrahedra. Zn, dark green; S, yellow; C, gray; O, red; N, dark blue; H, white.

more regular than in **1**, with similar bond lengths for the bidentate Zn1A−S1A (2.370 Å) and the bridging Zn1A−S1B (2.348 Å) bonds (Figure 3b, Table 3). The Zn1A−S1B−Zn1B angle is 92.75° and the S1A−Zn1A−S1B angle 124.27°. The substructure is slightly less planar than the Cd equivalent with a dihedral angle S1A−Zn1A−S1B−Zn1B of 163° (Figure 3b).

The distorted Zn tetrahedra[75] are linked into chains by sharing S atom corners. The other two corners of the tetrahedron are locked by N and O atoms, which limits the dimensionality to 1D. As in **1**, the chains mutually saturate the coordination sphere of their Zn centers by connecting to one another via the carboxylate functions (Figure 4a), but in **2** the carboxylates solely bind to chains *not* formed by their parent cysteine molecule. The arrangement of neighboring chains relative to the original one corresponds to the 2_1 screw axes along *b* and *c*. As in **1**, all chains are thus aligned along the *a* axis with angles of 90.6° between neighboring chains (Figure 3c and Figure 4).

In **2**, the substructure is close to a distorted ZnS würtzite structure with angles along the chains of 92.75° (Zn1A−S1B−Zn1B) and 124.27° (S1A−Zn1A−S1B), while the corresponding angle is 109.51° in the würtzite bulk structure (Figure 3b and 3d). Zn−S bond lengths of 2.348 and 2.370 Å in **2** are extremely close to the bulk values (2.354 and 2.350 Å). Zn also remains four coordinate, as in the bulk structure. The zigzag ZnS chain can be viewed as a distorted 1D fragment of the bulk würtzite structure. The non-bonding Zn−S contact (Zn1A−S1C = 3.832 Å) is significantly longer than the Zn−S bonds.

It is interesting to note that the decrease in the coordination number of the metal from 6 (Cd) to 4 (Zn) manifests itself by a drastic change in the coordination mode of the bridging functions. Thiolates bind in a μ_3 mode in **1** and a μ_2 mode in **2** and thus contribute to a decrease of one unit of the coordination number. The carboxylates display a bidentate (1,3) syn-anti mode in **1** and are only monodentate in **2**, further decreasing the coordination number of the metal by one unit, accounting for the octahedron-based geometry of **1** and the tetrahedron-based geometry of **2**.

Synthesis and Characterization of 1 and 2 as Phase Pure Materials. **1** can be obtained as a pure phase in conditions slightly milder than those used to get single crystals suitable for crystal structure determination. By reaction of $Cd(NO_3)_2.4H_2O$, L-cysteine, and NaOH at pH = 5.85 in water at 80 °C only for 24 h, no yellow amorphous powder forms and **1** is obtained as a pure phase, as evidenced by the powder X-ray diffraction pattern, that matches the pattern simulated from crystal structure data (Supporting Information, Figure S1). Using sodium hydrogencarbonate, the material obtained is not phase pure, and the powder pattern shows an extra peak at a *d*-spacing of 3.78 Å. Lowering the synthesis pH to 5.5 is enough to generate a small amount of yellow decomposition product which is detected by analysis of the UV data.

Elemental analysis is in agreement with the crystal structure formula Cd(L-cysteinate) ($C_3H_5CdNO_2S$, M = 232.9, found C 15.40, H 2.17, N 6.01, Cd 47.95; calcd C 15.56, H 2.18, N 6.05, Cd 48.55). TGA shows a weight loss of 39% around 290 °C corresponding to the decomposition of **1** to CdS and organics (Supporting Information, Figure S3, expected weight loss 37.3%).

The UV−visible spectrum of **1** was determined using diffuse reflectance measurements. The raw reflectance data was converted into the Kubelka−Munk function.[76] The absorption spectrum (Figure 5, left) shows no absorbance in the visible region, but a sharp edge around 290 nm, a pattern that is reminiscent of the optical behavior of certain CdS nanostructures.[15,20] Bearing in mind that the structure

(75) S1A−Zn−S1B = 124.72°; S1A−Zn−N1 = 86.41°; S1A−Zn−O1 = 112.31°; S1B−Zn−O1 = 105.37°; S1B−Zn−N1 = 104.16°; N1−Zn−O1 = 124.48°.

(76) The Kubelka−Munk function is used for the analysis of diffuse reflectance spectra obtained from weakly absorbing samples $F(R) = (1 - R)^2/2R = k/s$, where R = diffuse reflectance, k = absorption coefficient, and s = scattering coefficient.

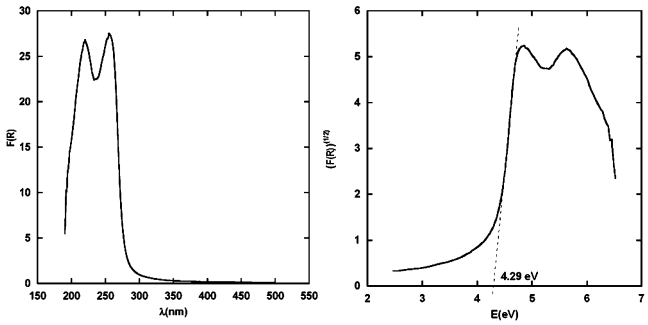

Figure 5. Optical absorption spectrum of **1** (left). Plot of $(F(R))^{1/2}$ as a function of the energy (right). Extrapolation of the linear section of the curve to the x axis gives the value of the band gap for an indirect transition. $F(R)$ is the Kubelka−Munk function $F(R) = (1 - R)^2/2R$, where R is the diffuse reflectance.

of **1** can be seen as a 1D fragment of the rock salt CdS phase, and the numerous examples of CdS nanostructures showing blue shifts of the band gap value up to 2 eV,[20] we evaluated the optical band gap of **1**. Along the sharp absorption edge, the energy band gap of a semiconductor can be determined via

$$\alpha = \text{const.}(h\nu - \text{Eg})^n, \qquad (1)$$

where α is the absorption coefficient, and Eg the band gap.[77] Depending on the transition mechanism, $n = 1/2$ for an allowed direct transition, $n = 3/2$ for a forbidden direct transition, and $n = 2$ for an indirect transition. We thus plotted $F(R)^{1/n}$ as a function of $h\nu$, for $n = 1/2$, 3/2, and 2, the Kubelka−Munk function $F(R)$ being proportional to α. Empirical fits of the curve give a band gap of 4.54 eV for $n = 1/2$, 4.37 eV for $n = 3/2$, and 4.29 eV for $n = 2$ by extrapolating the linear part of the graph to the energy axis (Figure 5, right). The electronic structure calculations discussed below show that **1** has an indirect gap. In this regard, we will consider the experimental band gap obtained for $n = 2$, which is 4.29 eV.

When irradiated above the absorption edge between 200 nm (the shortest accessible wavelength) and 260 nm, **1** showed no significant luminescence.

2 can be obtained as a pure phase in conditions similar to those used for **1**, by reaction of $Zn(NO_3)_2 \cdot 6H_2O$, L-cysteine, and NaOH in water at 80 °C for 24 h. The powder X-ray diffraction pattern is in agreement with the pattern simulated from crystal structure data (Supporting Information, Figure S4). As for **1**, phase purity is achieved by using sodium hydroxide instead of sodium hydrogencarbonate, and yellow amorphous decomposition products, detected by their contribution to the UV−visible spectra, are avoided by adjusting the pH to 5.9. Elemental analysis corresponds to the crystal structure formula Zn(L-cysteinate) ($C_3H_5ZnNO_2S$, M = 182.9, found C 19.38, H 2.70, N 7.55, Zn 34.89; calcd C 19.53, H 2.73, N 7.59, Zn 35.44). TGA shows a weight loss of 49% starting at 230 °C corresponding to the decomposition of **2** to ZnS and organics (Supporting Information, Figure S5, expected weight loss 47.5%).

(77) Pankove, J. I. *Optical processes in semiconductors*; Dover: New York, 1975.

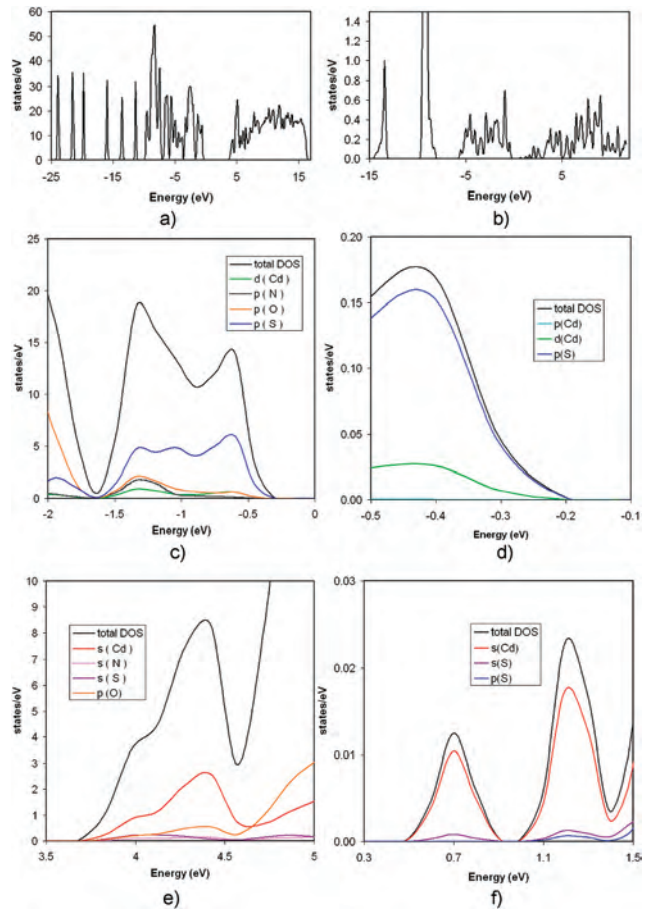

Figure 6. Calculated DOS for (a) **1**; (b) bulk CdS high pressure rock salt phase (lattice parameter fixed $a = 5.43$Å); (c) total DOS and elemental contributions on the edge of the valence band of **1**; (d) total DOS and elemental contributions on the edge of the valence band of rock salt CdS; (e) total DOS and elemental contributions on the edge of the conduction band of **1**; (f) total DOS and elemental contributions on the edge of the conduction band of bulk rock salt CdS. Full DOS and elemental contributions for **1** can be found in the Supporting Information, Figures S8, S9, and S10.

The UV−visible spectrum of **2** was determined using diffuse reflectance measurements. The spectrum (Supporting Information, Figure S6, left) shows no absorbance in the visible region, but a sharp edge around 260 nm. According to the calculations, **2** displays a direct gap and the experimental band gap, determined by the fit obtained for $n = 1/2$ (allowed direct transition), is 5.05 eV (in other cases, the evaluated gap is found to be 4.64 eV for $n = 2$ and 4.77 eV for $n = 3/2$, by extrapolating the linear part of the graph to the energy axis (Supporting Information, Figure S6, right)). **2** was irradiated above the absorption edge between 200 and 230 nm. As in the case of **1**, no significant luminescence was observed.

DOS Calculations. The calculated DOS for **1** (Figure 6a) allows us to evaluate a theoretical band gap of 3.98 eV (Supporting Information, Table S1). No single k-point was found to correspond to both the highest energy of the valence band and the lowest energy of the conduction band, indicating that the optical band edge transition must be phonon-assisted and that the gap is indirect.[78] The local arrangement of the 1D CdS substructures in **1**, the indirect nature of its gap, and its absence of luminescence are all reminiscent of

the bulk rock salt structure of CdS. The calculated value thus only slightly underestimates the experimental one (4.29 eV for an indirect transition). The underestimation of band gaps is a known shortcoming of DFT.[79] We also calculated the DOS of both the ambient pressure würtzite and high pressure rock salt CdS bulk phases. For würtzite bulk CdS, the previously described method was used. The calculated band gap is 1.70 eV, slightly higher than previously reported calculations,[79] but still smaller than the experimental value of 2.42 eV at room temperature (Supporting Information, Table S1). The lowest energy of the conduction band and the highest energy of the valence band correspond to the same k points[80] as expected for a direct gap system. We also performed DOS calculations on the parent rock salt high pressure phase of CdS. In this case, because of the metastable character of the phase, lattice parameters were fixed at the experimental value of $a = 5.43$ Å (at 40 kbar).[81] With this restriction, the atomic positions were optimized and used as an input to calculate the DOS. The gap was found to be 0.7 eV, smaller than the experimental value of 1.7 eV (Supporting Information, Table S1). The lowest energy of the conduction band and the highest energy of the valence band correspond to different k-points,[82] as expected for an indirect gap compound.[83] The calculations thus agree with the experimental finding that the gap increases as the Cd coordination number decreases—in further comparing the atom-based and molecule-based sources of the donor S atoms bridging the extended nets, the atomic parentage of the states defining the gap need to be considered.

A detailed study of the atomic parentage of the levels involved in the band edge transition in **1** reveals that the edge of the valence band is mostly composed of p orbitals of sulfur atoms (5.99 states/eV on p_S orbitals, 0.63 states/eV on p_O orbitals, 0.14 states/eV on p_N orbitals, 0.64 states/eV on d_{Cd} orbitals, at −0.6 eV, Figure 6c), while the s orbitals of cadmium give the main contribution to the levels on the edge of the conduction band (0.85 states/eV on s_{Cd} orbitals, 0.21 states/eV on s_S orbitals, 0.19 states/eV on p_O orbitals, 0.08 states/eV on s_N orbitals, at 4 eV, Figure 6e). The same pattern is observed in bulk rock salt CdS: the main contribution to the edge of the valence band is from p_S orbitals with 0.15 states/eV and d_{Cd} orbitals with 0.02 states/eV at −0.4 eV (Figure 6d), while the edge of the conduction band is composed essentially of s_{Cd} orbitals (0.01 states/eV at 0.7 eV) and s_S orbitals (0.0008 states/eV at 0.7 eV, Figure 6f). The same major contributions are observed on the edge of the gap in bulk würtzite CdS (Supporting Information, Figure S11). The electronic structure of the chalcogenide-derived unit in **1** is thus very similar in terms of the orbitals contributing to the band edge transition to that of bulk CdS, despite the molecular origin of the S moiety here. The p_S contribution on the edge of the valence band in **1** extends from −0.3 to −1.6 eV (1.3 eV wide) before becoming negligible. The equivalent contribution in the bulk CdS phases is spread over 5.5 eV (rock salt CdS) and 4.3 eV (würtzite CdS). The s_{Cd} contribution on the edge of the conduction band in **1** extends from 3.7 to 5.5 eV (1.8 eV wide) before becoming negligible, whereas in the bulk phase the spread is over 4.6 eV (rock salt CdS) and 4.2 eV (würtzite CdS), confirming that the energy widths of the p_S and s_{Cd} bands in **1** are significantly decreased by reduction of the S coordination number.

The same procedure was used to attempt to determine the DOS of **2**. In this case, the DFT optimized structure differs too strongly from the crystal structure to be considered a reliable model of **2** (Supporting Information, Figure S12). Cell parameters change from $a = 6.025(3)$ Å, $b = 8.838(5)$ Å, $c = 9.402(5)$ Å to $a = 6.32$ Å, $b = 9.91$ Å, $c = 10.21$ Å, showing a significant increase in *b* and *c*. Nevertheless, the coordination number, the first coordination sphere of Zn and the connectivity of L-cysteine remain similar, with acceptable bond lengths and angles in comparison with the experimentally determined structure (Supporting Information, Figure S13). The DFT-derived structure is less compact than the actual structure of **2**. In particular, the ZnS substructure is affected: the non bonding Zn−S contact along the *a* axis is extended by 15% and the folding angle of the chain along *a* increases by 10% (Supporting Information, Figure S12). This problem did not occur in **1**, owing to the tridentate and bridging coordination of cysteine which generates a constrained structure with denser packing. In **1**, no significant difference from the experimental structure is observed in the Cd−S bonds (less than 4.5% difference) and in the torsion angle of the ladder (0.5% difference, Supporting Information, Figure S7). In **2**, cysteine is only bidentate and gives the framework much more flexibility, as evidenced by the increase of the non bonding Zn1A−S1C contact from 3.832 Å to 4.218 Å (Figure 3b, Supporting Information, Figure S12). This can explain the expansion of the cell volume that is observed during optimization and also suggests that the isolated phase of **2** might be a metastable phase of Zn(L-cysteinate). Although no quantitative conclusion can be drawn from this specific calculation, qualitatively the DOS calculated for this system indicates that in both the crystal and DFT-optimized structures, the edge of the valence band is essentially developed on p_S orbitals and the edge of the conduction band on s_{Zn} and p_C orbitals, and both correspond to the same k point, consistent with an allowed direct transition at the band edge involving p_S and s_{Zn} orbitals.

Discussion

The metal−sulfur substructures in **1** and **2** can be considered as chains of CdS and ZnS in an environment slightly distorted with respect to the parent bulk structures (rock salt CdS and würtzite ZnS). As the source of the S

(78) The lowest energy of the conduction band in **1** corresponds to the k point (0.125 0.125 0.125), while the highest energy of the valence band can be found for k points (−0.375 0.125 0.125), (0.375 0.125 0.125), and (−0.375 −0.125 0.125).

(79) Kazume, N.; Takuya, S.; Yuta, M.; Mamoru, B.; Masayuki, H.; Taizo, S. *Phys. Rev. B: Condens. Matter* **2006**, *74*, 035210.

(80) (−0.125 0.125 0.125) and (0.125 −0.125 0.125).

(81) Owen, N. B.; Smith, P. L.; Martin, J. E.; Wright, A. J. *J. Phys. Chem. Solids* **1963**, *24*, 1519–1524.

(82) (0.0 0.0 0.0) corresponds to the lowest energy of the conduction band in **1**, while (0.4 0.4 0.0) corresponds to the highest energy of the valence band.

(83) Batlogg, B.; Jayaraman, A.; Van Cleve, J. E.; Maines, R. G. *Phys. Rev. B: Condens. Matter* **1983**, *27*, 3920–3923.

atom defining these substructures is purely molecular, the resulting coordination environments are imposed by the ligand bearing these atoms and can differ in significant respects from the stable bulk ambient pressure subunits previously found in chalcogenide hybrid structures.

In the bulk würtzite phase of CdS and ZnS which is stable at ambient pressure, both sulfur and metal atoms have a coordination number of 4 in a tetrahedral environment. In the high pressure phase of CdS (rock salt), the coordination number is increased to 6 (octahedral environment), which broadens the valence and conduction bands and reduces the band gap. In the CdS fragment of **1**, each Cd atom (respectively S atom) binds three S atoms (respectively Cd atoms) in a *mer* fashion. Considering a fragment of bulk rock salt CdS in this idealized topology, where the coordination number is reduced to 3, an increase of the band gap with respect to the bulk rock salt phase is expected because of the reduced number of near neighbor Cd−S interactions contributing to the bandwidth. In the ZnS fragment of **2**, each Zn atom (respectively S atom) binds two S atoms (respectively Zn atoms) in an arrangement similar to that of the bulk würtzite phase. In **2**, the reduced coordination number (there are only two S atoms in the tetrahedral coordination sphere of Zn) also increases the band gap (5.05 eV) compared to bulk würtzite ZnS (3.68 eV) where each Zn center is surrounded by four S atoms in a tetrahedral environment.

Examples of nanostructures of II−VI semiconductors based on fragments of the tetrahedral-based bulk structure showed that a blue shift of the band gap with respect to the corresponding bulk material arises from the decreased dimensionality of the II−VI systems.[2,13] This has been particularly well evidenced by Li and co-workers where the thickness of the layer in [(MQ)(L)] and [(M_2Q_2)(L)] bidimensional materials (M = Zn, Cd; Q = S, Se; L = R-NH_2), formed by sulfide synthesis in the presence of linker ligands, controls the band gap.[20] [(M_2S_2)(L)] bilayers, where metal centers are 4 coordinate (surrounded by four S atoms in the core of the bilayers or three S and one N atom on the edge) give band gaps of 2.9 eV (M = Cd) and 4.0 eV (M = Zn), while the blue shift is higher for monolayers, where metal centers are surrounded by three S and one N atom (band gap is 4 eV for M = Cd and 4.5 eV for M = Zn). The reduction of the number of S atoms in the coordination sphere of metal (from four in the bulk phase) because of the decreased dimensionality increases the band gap. Isolated 1D zigzag chain substructures are observed in ZnTe systems[18] with propanediamine as a chelate ligand—the decreased dimensionality from a 2D monolayer to a chain increases the band gap by 0.3 eV. Unlike these hybrid chalcogenides, where S atoms are present as sulfide S^{2-}, as in the bulk phases, the sulfur atoms in **1** and **2** are part of a molecular species, the cysteine ligand, and are engaged in coordination through a thiolate function. DOS calculations for **1**, **2**, and the CdS and ZnS bulk phases show that, despite the molecular nature of sulfur in **1** and **2**, the electronic structure generated on the edges of the band gap is formally comparable to that observed in parent bulk metal sulfide.

The DOS at the edge of the valence band in **1** is predominantly from p_S orbitals, while the DOS on the edge of the conduction band is essentially based on s_{Cd} orbitals. The contribution of atoms other than S on the edge of the valence band of **1** is extremely weak. This pattern is identical to that observed in both CdS bulk phases (würtzite and rock salt). A band edge optical transition (between p_S and s_{Cd} states) in **1** corresponds to a change in wavevector and thus needs to be phonon assisted, giving the indirect gap behavior found for the high pressure bulk CdS rock salt phase—the würtzite phase of CdS displays a direct gap electronic structure. This result illustrates the relationship between **1** and the rock salt phase of bulk CdS—the Cd is in a six coordinate environment with a *mer* arrangement of electronic structure-determining S donors that corresponds more closely to the high pressure than the ambient pressure tetrahedrally coordinated polymorph of CdS. This arrangement is enforced by the tridentate nature of the chelating amino acid ligand.

The value of the optical band gap determined for **1** (4.29 eV for an indirect transition) corresponds to a blue shift of 2.59 eV with respect to the high pressure rock salt phase of CdS (Supporting Information, Table S1). Referring to the würtzite phase of bulk CdS, the observed blue shift is 1.87 eV and represents an increase of 0.29 eV of the band gap with respect to the corresponding [(CdS)(L)] 2D monolayer (Supporting Information, Table S1),[20] although it should be noted that the Cd coordination is tetrahedral here.[20] In a two-atom thick [(CdS)(L)] monolayer, where the number of S neighbors for Cd is also three (as in **1**) in a tetrahedral environment, the blue shift with respect to the bulk phase is less important than in the 1D substructure of **1** because of the less pronounced bandwidth reduction due to the extent of Cd−S connectivity. **2** shows a blue shift of the band gap of 1.37 eV with respect to the bulk würtzite phase of ZnS and displays an increase of 0.55 eV with respect to the [(ZnS)(L)] 2D monolayer.[20]

1 displays a local structure reminiscent of the rock salt phase of CdS, with an electronic structure and optical properties related to this CdS bulk phase. In **2**, the local arrangement of metal and sulfur atoms is a distorted 1D fragment of the bulk würtzite phase, and the decrease of the ZnS system dimensions manifests itself by a blue shift of the absorption edge.[4,5,8] The magnitude of the blue shifts observed in **1** and **2** is in agreement with the trends observed by decreasing dimensionality from bulk to 2D, then to 1D structures.[20] The double role of L-cysteine, as a capping ligand, reducing the semiconductor dimensionality, and as a bridging ligand, connecting the substructures, produces a periodic array of uniform semiconductor nanostructures in a one pot reaction. This regular organization is usually difficult to achieve as most nanoparticles and nanostructures are polydisperse and subsequently difficult to organize in such a way. Nanoclusters (OD) can be organized uniformly and periodically,[84,85] but 1D or 2D examples of periodic arrangements are rather scarce.[20]

Conclusion

Under mild solvothermal conditions, we isolated 1D organo-functionalized blocks of II−VI semiconductors CdS and ZnS, where the chalcogenide is not elemental or isolated but part of a multidentate thiolate ligand. In the Cd case, the chelating nature of the ligand enforces an unusual *mer* arrangement of S neighbors found in the high-pressure polymorph of CdS. Despite the participation of S valence orbitals in C−S bonding within the ligand, the electronic structure of the extended molecule-based solids is strongly reminiscent of the pure semiconductor in terms of the orbital parentage of the states determining the band gap. The remaining functional groups of the thiol-bearing ligand are able to arrange these chalcogenide structures into chiral regular extended arrays. The organic capping ligand L-cysteine controls the dimensionality of the CdS and ZnS arrangement, but also, as a bridging ligand, organizes those substructures in a regular periodic fashion within the crystal. L-cysteine has been used for the synthesis of semiconductor nanoparticles with or without another source of sulfur, its role being to cap the nanoparticles.[41,71,86−89] This suggests that **1** and **2** might be intermediate species formed during synthesis of those CdS and ZnS nanostructures that help limiting their growth. **1** and **2** are chiral d^{10} systems with high UV transparency, motivating further studies of their optical properties.[90,91]

Acknowledgment. We thank the EPSRC for funding under EPSRC/C511794 and for access to the SRS, and the Leverhulme Trust for support of JNR. We thank the Royal Society for a Wolfson Research Merit Award to M.J.R. We thank Dr John E. Warren for support on station 9.8 at the SRS. We are grateful to G. Kresse for supplying a prerelease of vasp.5.1 and to Helen Williams for assistance with some of the calculations.

Supporting Information Available: Powder X-ray diffraction patterns, TGA curves, UV−vis spectra, total and elemental DOS graphs for **1** and greenockite CdS (würtzite phase), comparative views of the crystal and optimized structures of **2**. This material is available free of charge via the Internet at http://pubs.acs.org.

IC801097W

(84) Zheng, N.; Bu, X.; Lu, H.; Zhang, Q.; Feng, P. *J. Am. Chem. Soc.* **2005**, *127*, 11963–11965.
(85) Zhang, Q.; Bu, X.; Zhang, J.; Wu, T.; Feng, P. *J. Am. Chem. Soc.* **2007**, *129*, 8412–8413.
(86) Kho, R.; Torres-Martinez, C. L.; Mehra, R. K. *J. Colloid Interface Sci.* **2000**, *227*, 561–566.
(87) Chen, J. L.; Zhu, C. Q. *Anal. Chim. Acta* **2005**, *546*, 147–153.
(88) Chatterjee, A.; Priyam, A.; Bhattacharya, S. C.; Saha, A. *J. Lumin.* **2007**, *126*, 764–770.
(89) Xu, R.; Wang, Y.; Jia, G.; Xu, W.; Liang, S.; Yin, D. *J. Cryst. Growth* **2007**, *299*, 28–33.
(90) Sankar, R.; Raghavan, C. M.; Mohan Kumar, R.; Jayavel, R. *J. Cryst. Growth* **2007**, *305*, 156–161.
(91) Dhanuskodi, S.; Vasantha, K.; Mary, P. A. A. *Spectrochim. Acta, Part A* **2007**, *66*, 637–642.